VSP

Advanced Powder Technology 19 (2008) 293–306

Advanced Powder Technology
www.brill.nl/apt

Original paper

Solidification Mechanism of the Sediment Formed by Particle Settling — Analysis of the Final State of the Sediment

Hiroshi Satone *, **Takehiro Mamiya**, **Asami Harunari**, **Takamasa Mori and JunIchiro Tsubaki**

Department of Molecular Design and Engineering, Graduate School of Engineering, Nagoya University, Furo-cho, Chikusa-ku, Nagoya 464-8603, Japan

Received 29 May 2007; accepted 26 July 2007

Abstract

Particles in a slurry often form a solidified layer at the bottom of its container, making the slurry no longer useable in material fabrication processes. In order to analyze the mechanism of solidification of a sediment, we observed the gravitational sedimentation behavior of various slurries prepared by changing the slurry pH and measured the height of the solidified layer after settling by inclining the test tube. We conclude that the height of the solidified layer has a close correlation with the maximum repulsive force calculated by the DLVO theory, but not with the potential barrier. In addition, we can express the final height of the solidified layer using a very simple model.

Keywords

Slurry, sedimentation, solidification, DLVO theory, maximum repulsive force, potential barrier.

Nomenclature

V_R	electrostatic repulsion potential	(J)
x	particle diameter	(m)
r	distance between particle surfaces	(m)
N_A	Avogadro's number	(–)
Z_i	valence of ion	(–)
C_i	ion concentration	(mol/l)
k	Boltzmann constant	(J/K)
T	temperature	(K)

* To whom correspondence should be addressed. E-mail: satone@nagoya-u.jp

 DOI:10.1163/156855208X294645

V_A	van der Waals potential	(J)
A	Hamaker constant	(J)
V_t	total interaction potential	(J)
F_t	interaction force between particles	(N)
F	force resulting from the weight of one particle	(N)
n	maximum number of particles	(–)
F_{max}	maximum repulsive force	(N)
$h_{cal,c}$	calculated value of the depth of the flowable layer in case of cubic arrangement without correction	(m)
h_{cal}	calculated value of the final depth of the flowable layer	(m)
g	gravitational acceleration	(m/s^2)

Greek

ε_r	relative permittivity	(–)
ε_0	permittivity of vacuum electric constant	(F/m)
ψ_0	surface potential	(V)
κ	Debye–Huckel parameter	(–)
ρ_p	particle density	(kg/m^3)
ρ_f	liquid density	(kg/m^3)
Φ_s	final packing fraction of the sediment	(–)

1. Introduction

In various industrial processes, such as wet shape forming of ceramics, spray drying granulation and film formation, fine particles are usually applied in a slurry (fine particles dispersed in a dispersion medium). After concentration, dehydration and drying, the slurry becomes a final product. It is very important to evaluate slurry characteristics to predict the product characteristics. Conventionally, slurries were mainly evaluated by measuring their apparent viscosities. However, it has been reported that the apparent viscosity of a slurry does not have a good relationship with the packing fraction of green bodies [1–5]. Therefore, product characteristics cannot be controlled by apparent viscosity alone.

As a result, many studies have evaluated the packing characteristics of particles in slurries using gravitational settling tests [6–16]. However, it takes several hours to perform experiments even when using centrifugal force. Therefore, a quicker and easier evaluation of slurry properties is desirable for industrial applications.

In our previous reports, we proposed an evaluation method to predict in a short time the packing characteristics of a slurry by measuring the hydrostatic pressure of the slurry at the base of a settling tube [17–19], and proposed a method that could easily predict the average packing fraction of cake and the packing fraction distribution by constant pressure filtration [20–22].

In these reports, we evaluated alumina slurries, which were prepared under various pH conditions, using hydrostatic pressure measurement. In the case of a slurry with pH 4.0, in spite of the settling interface height being constant, the hydrostatic

pressure did not fall to a minimum. This shows that some of the particles in the sediment have flowability. On the other hand, in the case of a slurry with pH 6.0 near the isoelectric point, the hydrostatic pressure fell immediately and this sediment solidified.

Furthermore, the slurry could be concentrated without forming cake by adding dispersant instead of flocculant used for conventional solid–liquid separation operations. In addition, the concentrate, having maintained flowability, was obtained continually without a mechanical hand-scraping device [23, 24].

In field application of slurries, the following problem occurred. Generally, large quantities of slurries are made at a time and stored for a long time in a container. During storage, the particles in the slurry often form a very hard solidified layer at the bottom of the container. In such a case, the slurry with the solidified layer is no longer usable in the material fabrication process.

In general, it is thought that the whole condensate solidifies. However, sometimes there is a flowable layer along with the solidified layer.

From these considerations, it is important to prevent the solidification of particles in order to maintain slurry properties. We thought that interaction forces acting between particles would have an effect on the formation of the solidified layer.

In this study, we observed the sediment in slurries with varying pH using gravitational settling experiments, calculated the interaction forces between particles with the DLVO theory [25], and analyzed the relationship between the solidification of the sediment and the interaction forces in the final state of the sediment.

2. Experimental

Slurries were prepared from abrasive alumina powder (JIS #6000; average particle size 2 μm, density 3.96 g/cm^3; Fujimi) and distilled water by ultrasonication. The solid concentration was 3 vol.%. Figure 1 shows the ζ potential as a function of the pH of alumina slurries. The ζ potential was measured using an electrophoresis analyzer (Model Mark II; Rank Brothers). The values of the slurry pH were changed using HCl (Wako). In order to control the interaction forces between particles, salt concentrations were changed using NaCl (Wako). The slurry conditions are summarized in Table 1. The prepared slurries were poured into acrylic test tubes with a diameter of 20 mm. The initial height of each of the slurries was 150 mm. The top of the tube was hermetically sealed with a film. After preparation, the particles in the slurry underwent gravitational settling. In order to confirm repeatability, several settling tubes poured from the same slurry were prepared. When the position of the interface between the solidified and the flowable layer in a slurry became constant, this was considered to mark the end of sedimentation and the depth of the flowable layer was measured. The depth of the flowable layer was obtained as follows. First, the height of the sediment was measured. Second, the height of the solidified layer was measured by inclining the test tube. The depth of the flowable layer was obtained by subtracting the latter from the former, as shown in Fig. 2.

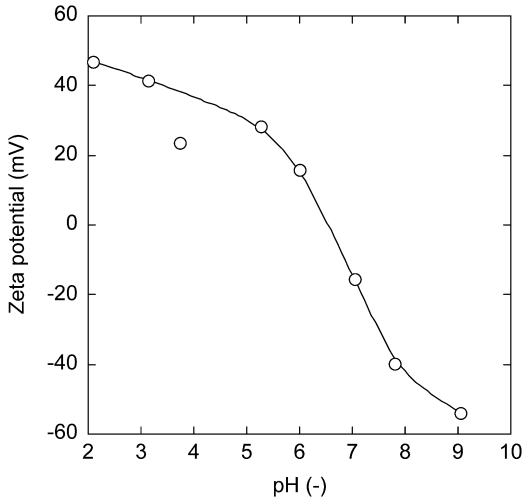

Figure 1. Zeta potential of abrasive alumina powder as a function of pH.

Table 1.
Total ion concentration and ζ potential of prepared slurries

Number	pH	Total ion concentration $\times 10^3$ (mol/l)	ζ (mV)
1	3.7	2.34	39.2
2	4.0	1.00	37.4
3	4.0	2.47	37.4
4	4.0	3.27	37.4
5	4.0	3.90	37.4
6	4.3	1.88	35.4
7	4.3	1.91	35.4
8	4.3	3.05	35.4
9	4.4	2.15	34.7
10	4.5	1.68	33.9
11	4.5	2.78	33.9
12	4.7	3.26	32.4
13	5.0	1.19	29.7
14	5.0	2.31	29.7
15	5.2	3.11	27.8
16	5.5	2.07	24.4
17	5.5	3.00	24.4
18	5.6	0.80	23.1
19	6.0	0.80	17.0
20	6.0	1.97	17.0

In gravitational settling experiment of slurries, the height of the sediment and the packing fraction ($\Phi_s = 0.64$) were the same for all slurries. At first glance,

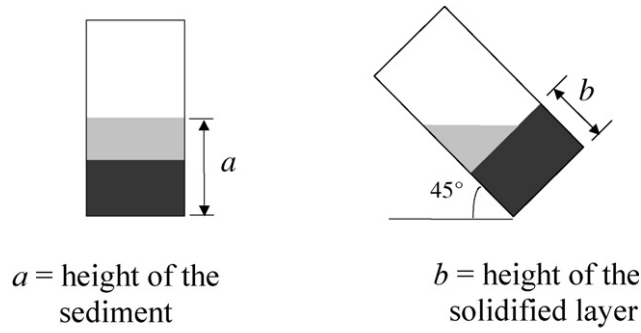

Figure 2. Measurement method of the depth of the flowable layer.

there were no clear differences in the preparation conditions of the slurries. In the sediment for all slurries, there was a solidified layer on the bottom and a flowable layer above it. Figure 3 shows images of the sediment observed by a digital camera. Figure 3 shows that although there was no difference in appearance of the sediments prepared by different slurry conditions, there were differences in the heights of the solidified layers. The sediments did not have clear supernatants for all slurries because of the presence of very small particles. The amount of the particles was very small and it was assumed that they did not influence the analysis of the sediment. In order to observe the time change of the solidified layer, a slurry was poured into several test tubes and then each tube was inclined at arbitrary times to obtain the values of the depth of the flowable layer. Slurries used in this experiment were prepared in three different typical conditions. Figure 4 shows the time change of the depth of the flowable layer. The depth of the flowable layer did not change after the end of sedimentation. Therefore, the value of the depth of the flowable layer after 72 h was used for analysis.

3. Results and Discussion

In the DLVO theory, the total interaction potential V_t expressed by (1) is defined as the sum of electrostatic repulsion potential V_R expressed by (2) and van der Waals potential V_A expressed by (3):

$$V_t = V_R + V_A \tag{1}$$

$$V_R = \pi\varepsilon_r\varepsilon_0 x\psi_0^2 \ln[1 + \exp(-\kappa r)]$$

$$\kappa = \left(\frac{1000N_A \sum Z_i C_i e^2}{\varepsilon_r\varepsilon_0 kT}\right)^{0.5} \tag{2}$$

$$V_A = -\frac{Ax}{24r}. \tag{3}$$

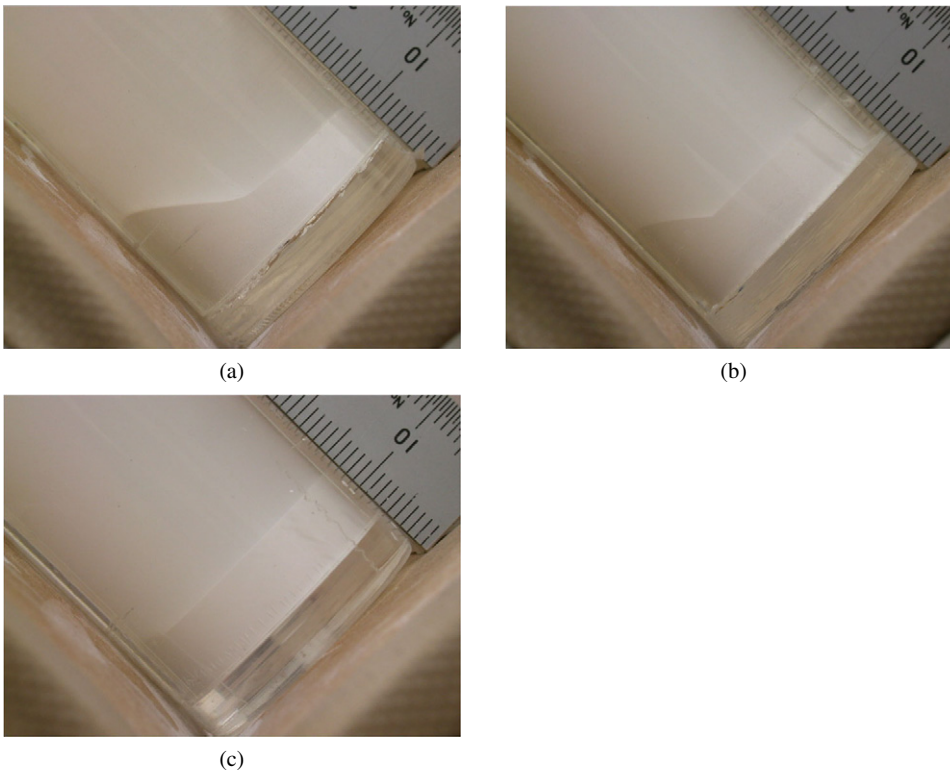

(a) (b)

(c)

Figure 3. Difference of sediments in the inclining test tube observed by a digital camera. (a) No. 7; (b) No. 13; (c) No. 19. This figure is published in color on http://www.ingentaconnect.com/content/vsp/apt

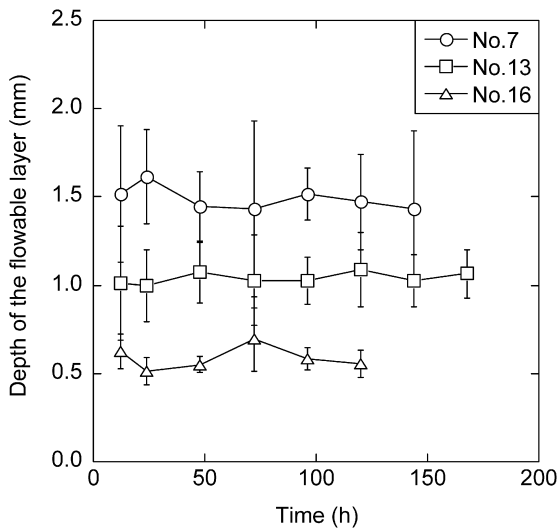

Figure 4. Time change of the depth of the flowable layer.

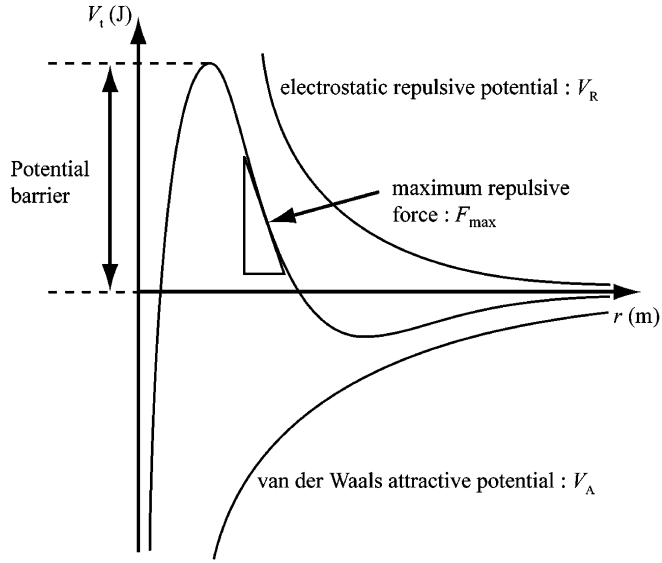

Figure 5. Schematic representation of the potential curve according to the DLVO theory.

In (3), it is necessary that a particle is a sphere having a smooth surface in comparison with the extent where the van der Waals force influences. Although the particles used in this study are not completely sphere and smooth, we did not consider it and use (3) for simplification of the calculation. Figure 5 shows a schematic representation of the potential. The potential barrier is defined as the local maximum value in the potential curve as shown in Fig. 5. Generally, particles in a slurry retain a good dispersion state when the potential barrier is more than 15–25 kT [25, 26]. In addition, the interaction force F_t, the differential of the potential curve, is expressed by:

$$F_t = -\frac{dV_t}{dr}. \tag{4}$$

The interaction force between particles is repulsive for positive values and attractive for negative values. Figure 6 shows examples of potential curves of slurries prepared in this study. A test result for the ζ potential was substituted for surface potential ψ_0. As shown in Fig. 6, the potential barrier and the repulsive force have been affected by the preparation conditions. Here, the maximum value of the repulsive force was defined as the maximum repulsive force F_{max}.

Figure 7 shows the relationship between the depth of the flowable layer and the potential barrier, and Fig. 8 shows the relationship between the depth of the flowable layer and the maximum repulsive force. Straight lines in Figs 7 and 8 are regression lines provided by the least-squares method. The R^2 value for the regression lines was 0.83 when the variable was the potential barrier (Fig. 7) and 0.94 when the variable was the maximum repulsive force (Fig. 8). Both of potential barrier and the maximum repulsive force have a correlation with the depth of the flowable layer;

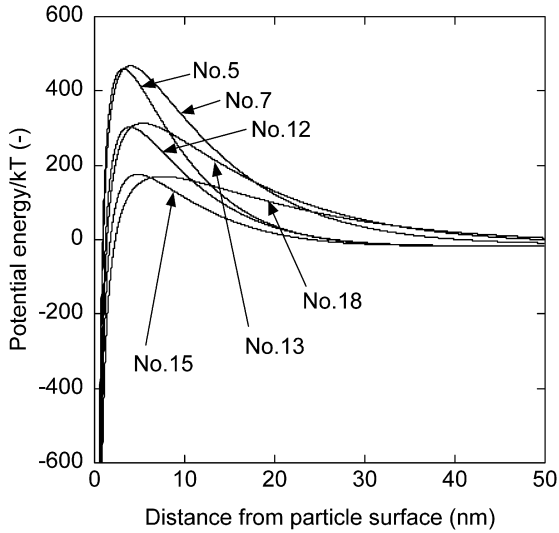

Figure 6. Examples of potential curves of prepared slurries.

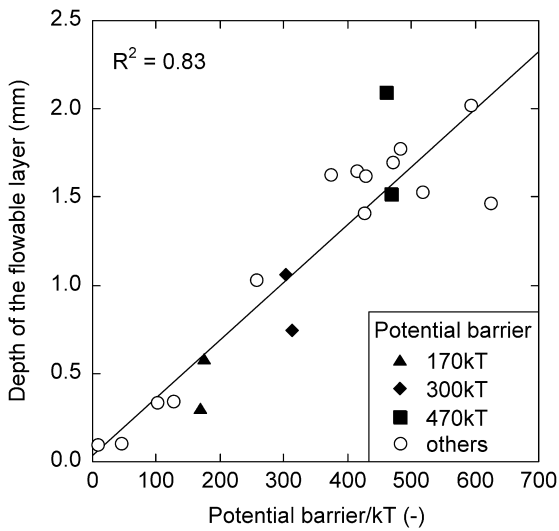

Figure 7. Relationship between the depth of the flowable layer and the potential barrier.

however, the latter has a better correlation. Miyahara *et al.* [27] obtained a similar result that the determinant factor for the order formation is not potential, but force-acting particles in absorption phenomenon between the nanoparticle and substrate.

To explain this, Fig. 9 shows the relationship between the potential barrier and the maximum repulsive force. As the interparticle potential is expressed by (1) and the maximum repulsive force between particles is expressed by (4), they are correlated and cannot be changed independently. We focus our attention on the points that have approximately the same potential barrier but different maximum repulsive forces:

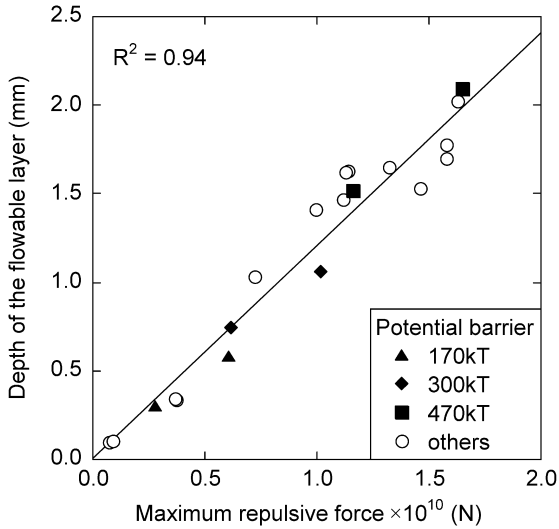

Figure 8. Relationship between the depth of the flowable layer and the maximum repulsive force.

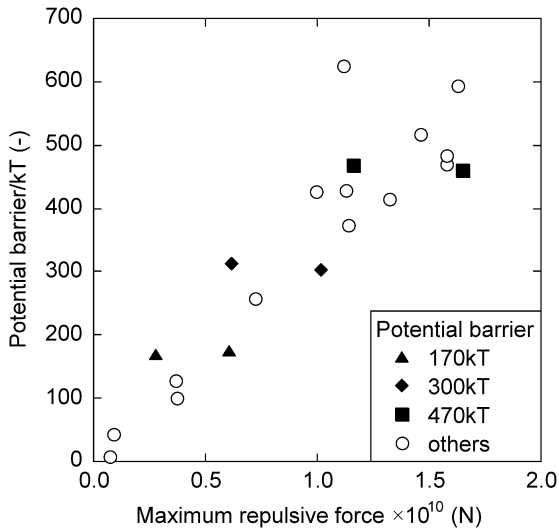

Figure 9. Relationship between the potential barrier and the maximum repulsive force.

about 470 kT (nos 5 and 7; ■), about 300 kT (nos 12 and 13; ◆) and about 170 kT (nos 15 and 18; ▲), as shown in Fig. 6. In Fig. 8, these points are distributed near the regression line. In Fig. 7, each two points having the same potential barrier are plotted vertically because the axis of the abscissas is a potential barrier. From these results, we thought that this phenomenon should be discussed based on the maximum repulsive force.

Therefore, we discuss the influence of the maximum repulsive force on solidification of the sediment and its flowability. Here, we define 'attach' as the state that

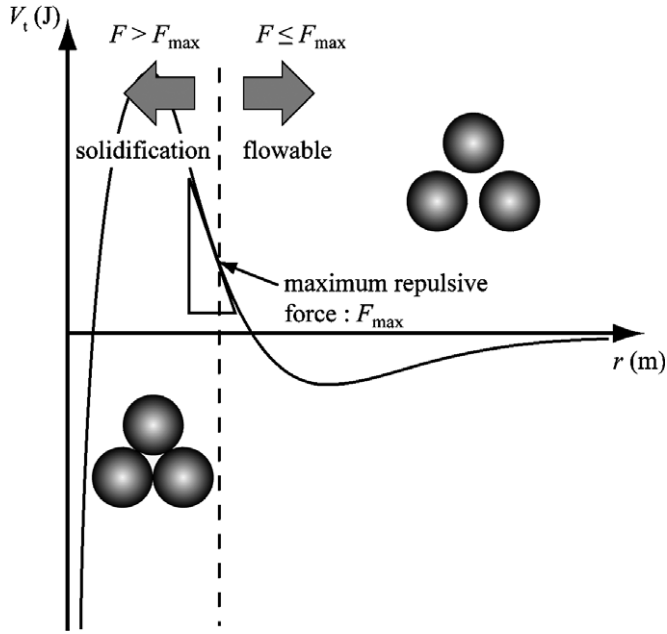

Figure 10. Schematic representation of the effect of the maximum repulsive force on solidification of the particles in the sediment.

a particle overcomes the potential barrier and solidifies, and 'contact' as the state that a particle does not overcome the potential barrier, but the distance between two particle surfaces is very close and particle interaction force acts. The gravitational force between the particles, the repulsive force between the particles and the fluid drag force acting on the particles should be considered when examining the settling particles or the sedimentation process. Among these forces, the driving force of solidification of the sediment is the gravitational force between the particles. On the other hand, the repulsive force and the fluid drag force act as resistance forces in solidification.

After the settling has started, the particles in the slurry continue to settle until they arrive at the top of the sediment. When the particle was close to the sediment, it was determined whether the particle attached others and solidified or not, using the relationship between driving force and resistance force. Figure 10 shows a schematic representation of the effect of the maximum repulsive force on solidification of the particles in the sediment. When the driving force is smaller than or equal to the resistance force, the particles are not able to attach each other. Under these conditions, the sediment retains flowability. On the other hand, if the driving force is greater than the resistance force, the particles can overcome the potential barrier, reach the primary minimum point and attach other particles. Under this condition, the sediment solidifies because of the strong attractive force acting between particles.

Based on this idea, we tried to calculate the depth of the flowable layer in the sediment from the maximum repulsive force. For calculation, it is necessary to assume a packing structure of the sediment. We considered general packing structures such as body-centered cubic (b.c.c.), face-centered cubic (f.c.c.), hexagonal close packed (h.c.p.) and cubic structure. For these arrangements, except the cubic arrangement, a particle has more than three contact points. When the driving force is greater than the resistance force, i.e., a particle is going to attach, a particle overcomes the potential barrier at each point at the same time. Here, the force between particles is distributed and is not homogeneous in the real sediment. Therefore, it is hard to think that a particle overcomes the potential barrier at the same time at each point. That is, it is supposed that particles in the solidified layer attach each other at two points. For trial, we calculated in the case of b.c.c., f.c.c. and h.c.p., that the calculated depth of the flowable layer was much larger than the experimental value. From these, for modeling the sediment structure, b.c.c., f.c.c. and h.c.p. are not suitable, but cubic arrangement is because it has two contact points.

Figure 11 shows a schematic illustration of the particle sedimentation model. For simplification, we made following three assumptions. First, the particles are spherical and monodispersed. Second, the particle arrangement in the sediment is cubic in structure. Third, the particles at the bottom of the sediment are unable to move.

The force F resulting from the weight of one particle is expressed by (5), using particle diameter x, particle density ρ_p and liquid density ρ_f:

$$F = \frac{\pi}{6} x^3 (\rho_p - \rho_f) g. \tag{5}$$

Here, a certain particle inside the sediment is considered. The particle receives a downward force because of the weight of particles above it, and an upward force because of the repulsive forces between it and the particles below it. The maximum number of particles n that can be supported by the maximum repulsive force between particles can be expressed using F and F_{max} by:

$$n = \mathrm{int}\left(\frac{F_{max}}{F}\right). \tag{6}$$

The top n particles have flowability because of the maximum repulsive force between particles. From the $(n+1)$th particle, the particles attached with each other and solidified. Therefore, the depth of the flowable layer is expressed by the following equation:

$$h_{cal,c} = nx. \tag{7}$$

However, the final packing fraction of the sediment, Φ_s, obtained from experiments was 0.64. This is about 20% higher than that of a cubic arrangement, 0.52, assumed in the calculation. Therefore the calculated value of the depth of the flowable layer in the case of a cubic arrangement was corrected by the packing fraction obtained from the experiment. This value was defined as the calculated value of the

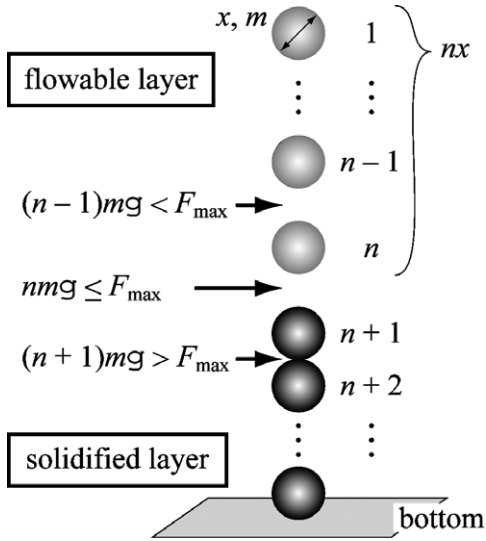

Figure 11. Schematic illustration of the particle sedimentation model.

final depth of the flowable layer, h_{cal}, expressed by:

$$h_{\mathrm{cal}} = \frac{0.52}{\Phi_{\mathrm{s}}} \cdot nx = 0.81 \cdot \mathrm{int}\left(\frac{F_{\max}}{F}\right) \cdot x$$
$$= 0.81 \cdot \mathrm{int}\left(\frac{F_{\max}}{\frac{\pi}{6}x^3(\rho_{\mathrm{p}} - \rho_{\mathrm{f}})g}\right) \cdot x. \tag{8}$$

Figure 12 shows a comparison between the calculated and experimental values for the depth of the flowable layer. The broken line in Fig. 12 is the value calculated using (7) and the solid line is the value calculated using (8). From Fig. 12, the values calculated using (8) agree fairly well with the experimental results. From these results, we can estimate the depth of the flowable layer using the maximum repulsive force determined by the DLVO theory.

4. Conclusions

In order to discuss the mechanism of solidification of sediment, the sediment obtained from gravitational settling experiments was observed using slurries prepared by changing the pH value. The following results were obtained:

(i) All the sediments obtained in the slurries consisted of a solidified layer and a flowable layer.

(ii) We can estimate the depth of the flowable layer from a particle sedimentation model using the maximum repulsive force determined by the DLVO theory.

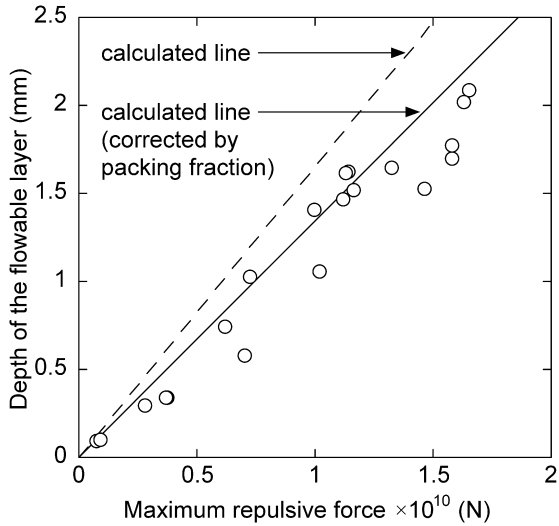

Figure 12. Comparison between calculated and experimental values of the depth of the flowable layer.

Acknowledgment

The authors wish to thank Mr Shinji Torii for supporting the experiments.

References

1. B. V. Velmakanni, J. Chang, F. Lange and D. Pearson, New method for efficient colloidal particle packing via modulation of repulsive lubricating hydration forces, *Langmuir* **6**, 1323–1325 (1990).
2. J. Davies and J. G. P. Binner, The role of ammoniumpolyacrylate in dispersing concentrated alumina suspensions, *J. Eur. Ceram. Soc.* **20**, 1539–1553 (2000).
3. J. J. Guo and J. A. Lewis, Effect of ammonium chloride on the rheological properties and sedimentation behavior of aqueous silica suspensions, *J. Am. Ceram. Soc.* **83**, 266–272 (2000).
4. J. Tsubaki, M. Kato, M. Miyazawa, T. Kuma and H. Mori, The effects of the concentration of a polymer dispersant on apparent viscosity and sedimentation behavior of dense slurries, *Chem. Eng. Sci.* **56**, 3021–3026 (2001).
5. R. R. Ramachandra, H. N. Roopa and T. S. Kannan, Effect of pH on the dispersability of silicon carbide powders in aqueous media, *Ceram. Int.* **25**, 223–230 (1999).
6. D. C. Dixon, P. Souter and J. E. Buchanan, A study of inertial effects in sedimentation, *Chem. Eng. Sci.* **31**, 737–740 (1976).
7. E. M. Tory and D. K. Pickard, Extensions and refinements of a Markov model for sedimentation, *J. Math. Anal. Applic.* **86**, 442–470 (1982).
8. G. C. Barker and M. J. Grimson, Theory of sedimentation in colloidal suspensions, *Colloids Surfaces* **43**, 55–66 (1990).
9. J. Tsubaki, Y. Yoshida, M. Shikata, H. Mori, T. Yokoyama and M. Naito, New slurry characterization technique for optimizing wet-shaping process (part 1): transient centrifugal consolidation process of particulate slurries, *J. Ceram. Soc., Japan* **106**, 504–508 (1998).

10. J. Tsubaki, H. Mori, M. Kato, K. Okuta, Y. Yoshida and T. Yokoyama, New slurry characterization technique for optimizing wet-shaping process (part 2): dependency of centrifugal effect on slurry consolidation process, *J. Ceram. Soc., Japan* **106**, 616–620 (1998).
11. R. Bürger, Phenomenological foundation and mathematical theory of sedimentation–consolidation processes, *Chem. Eng. J.* **80**, 177–188 (2000).
12. J. Tsubaki, H. Mori and T. Sugimoto, Network formation mechanism of fine particles in suspension. Simulation on the influence of particle bridging, *J. Soc. Powder Technol., Japan* **37**, 92–99 (2000).
13. T. Sugimoto, H. Mori and J. Tsubaki, Network formation mechanism of fine particles in suspension. Simulation on the structure formation in binary dispersions, *J. Soc. Powder Technol., Japan* **37**, 100–106 (2000).
14. T. Sugimoto, H. Hirose, H. Mori and J. Tsubaki, Analysis of settling interface formation process in suspension, *J. Soc. Powder Technol., Japan* **38**, 11–17 (2001).
15. C. P. Chu, S. P. Ju, D. J. Lee and K. K. Mohanty, Batch gravitational sedimentation of slurries, *J. Colloid Interface Sci.* **245**, 178–186 (2002).
16. H. Kim, T. Mori and J. Tsubaki, Effects of solid concentration and dispersant dosage on sedimentation behavior, *J. Soc. Powder Technol., Japan* **41**, 656–662 (2004).
17. J. Tsubaki, K. Kuno, I. Inamine and M. Miyazawa, Analysis of sedimentation and settling process of dense alumina slurries by hydrostatic pressure measurement, *J. Soc. Powder Technol., Japan* **40**, 432–437 (2003).
18. T. Mori, M. Ito, T. Sugimoto, H. Mori and J. Tsubaki, Slurry characterization by hydrostatic pressure measurement — effect of initial height on sedimentation behavior, *J. Soc. Powder Technol., Japan* **41**, 522–528 (2004).
19. T. Mori, K. Kuno, M. Ito, J. Tsubaki and T. Sakurai, Slurry characterization by hydrostatic pressure measurement-analysis based on apparent weight flux ratio, *Adv. Powder Technol.* **17**, 319–332 (2006).
20. J. Tsubaki, H. Kim, T. Mori, T. Sugimoto, H. Mori and N. Sasaki, New evaluation technique for slurry characterization by constant pressure filtration, *J. Soc. Powder Technol., Japan* **40**, 438–443 (2003).
21. H. Kim, T. Mori and J. Tsubaki, Development of slurry characterization method by constant pressure filtration, *J. Ceram. Soc., Japan* **113**, 761–767 (2005).
22. T. Mori, H. Kim, K. Ato and J. Tsubaki, Measuring packing fraction distribution in cake filtered under constant pressure and estimation from measured filtrate volume, *J. Ceram. Soc., Japan* **114**, 318–322 (2006).
23. J. Tsubaki and T. Mori, A powder operation born from characterization technique — development of a high performance cake-less continuous filtration system, *Funtai to Kougyo* **36**, 52–58 (2004).
24. J. Tsubaki, T. Mori, U. Tseveen and O. Bayanjargal, Development of a novel slurry condensation method by applying dispersant instead of flocculant, *J. Soc. Powder Technol., Japan* **43**, 731–736 (2006).
25. T. F. Tadros, *Handbook of Applied Surface and Colloid Chemistry*. Wiley, New York (2002).
26. K. Furusawa, *New Technology and Applications of Dispersion & Emulsion Systems*, pp. 116–117, Technosystem (2006).
27. M. Miyahara, S. Watanabe, Y. Gotoh and K. Higashidani, Adsorption and order formation of colloidal nanoparticles on a substrate: a Brownian dynamics study, *J. Chem. Phys.* **120**, 1524–1534 (2004).